arXiv:1305.5010v1 [hep-ph] 22 May 2013

Analysis of $B_s \to \phi\mu^+\mu^-$ decay within supersymmetry

Yuan-Guo Xu,   Li-Hai Zhou,   Bing-Zhong Li,   Ru-Min Wang*

College of Physics and Electronic Engineering, Xinyang Normal University, Xinyang, Henan 464000, China

October 7, 2018

Abstract

Motivated by the first measurement on $\mathcal{B}(B_s \to \phi\mu^+\mu^-)$ by the CDF Collaboration, we study the supersymmetric effects in semi-leptonic $B_s \to \phi\mu^+\mu^-$ decay. In our evaluations, we analyze the dependences of the dimuon invariant mass spectrum and the forward-backward asymmetry on relevant supersymmetric couplings in the MSSM with and without R-parity. The analyses show the new experimental upper limits of $\mathcal{B}(B_s \to \mu^+\mu^-)$ from the LHCb Collaboration could further improve the bounds on sneutrino exchange couplings and $(\delta_{LL}^u)_{23}$ as well as $(\delta_{LL,RR}^d)_{23}$ mass insertion couplings. In addition, within the allowed ranges of relevant couplings under the constraints from $\mathcal{B}(B_s \to \phi\mu^+\mu^-)$, $\mathcal{B}(B \to K^{(*)}\mu^+\mu^-)$ and $\mathcal{B}(B_s \to \mu^+\mu^-)$, the dimuon forward-backward asymmetry and the differential dimuon forward-backward asymmetry of $B_s \to \phi\mu^+\mu^-$ are highly sensitive to the squark exchange contribution and the $(\delta_{LL}^u)_{23}$ mass insertion contribution. The results obtained in this work will be very useful in searching supersymmetric signal at the LHC.

PACS Numbers: 13.20.He, 12.60.Jv, 11.30.Er

*E-mail: ruminwang@gmail.com

1 Introduction

Flavor changing neutral current (FCNC) processes can occur via penguin or box diagrams in the standard model (SM) and are very sensitive to the gauge structure as well as various extensions of the SM. So they can provide useful information on the parameters of the SM and test its predictions. Meanwhile, they can offer a valuable possibility of an indirect search of new physics (NP). The transition $b \to s\mu^+\mu^-$, for instance, is a FCNC process, present in the decays $B \to K\mu^+\mu^-$, $B \to K^*\mu^+\mu^-$, $B_s \to \phi\mu^+\mu^-$ and $B_s \to \mu^+\mu^-$. The rates for these decays could be changed by NP contributions, and this would consequently alter the dimuon invariant mass spectra and the forward-backward asymmetries for these semi-leptonic decays from the SM predictions.

Recently, the first measurements of the branching ratio [1] and the dimuon invariant mass spectrum [2] of $B_s \to \phi\mu^+\mu^-$ have been reported by CDF Collaboration. And its branching ratio is [2]

$$\mathcal{B}(B_s \to \phi\mu^+\mu^-) = (1.47 \pm 0.24 \pm 0.46) \times 10^{-6}, \tag{1}$$

which is quite consistent with its SM prediction $\mathcal{B}^{SM}(B_s \to \phi\mu^+\mu^-) = (1.48^{+2.06}_{-0.46}) \times 10^{-6}$. Moreover, the upper limit of $\mathcal{B}(B_s \to \mu^+\mu^-)$ has been significantly improved by the CDF, CMS and LHCb Collaborations [3–7]. The lowest published limit from the LHCb Collaborations at 95% confidence level (CL) is [8]

$$\mathcal{B}(B_s \to \mu^+\mu^-) < 4.5 \times 10^{-9}. \tag{2}$$

These observables are important to test the SM and constrain contributions of the possible NP models. Thus, these processes have attracted much attention (for instance, Refs. [9–15]).

In this paper, following closely the analyses of Ref. [16], we will study R-parity violating (RPV) supersymmetric effects and the R-parity conserving (RPC) mass insertion (MI) supersymmetric effects on the observables of $B_s \to \phi\mu^+\mu^-$ decay from the new experimental data in the minimal supersymmetric standard model (MSSM). Using the experimental limits on $\mathcal{B}(B_s \to \mu^+\mu^-)$ from LHCb [8], $\mathcal{B}(B \to K^{(*)}\mu^+\mu^-)$ from Particle Data Group [17] as well as $\mathcal{B}(B_s \to \phi\mu^+\mu^-)$ from CDF [2], we will constrain the relevant new couplings and examine the supersymmetric effects on the branching ratio, the dimuon invariant mass spectrum, the for-

ward backward asymmetry and the differential forward backward asymmetry of $B_s \to \phi\mu^+\mu^-$ decay.

The paper is arranged as follows. In Section 2, we briefly introduce the theoretical framework for $B_s \to \phi\mu^+\mu^-$ decay. In Section 3, we present our numerical analyses and discussions. Section 4 contains our conclusion.

2   The theoretical framework of $B_s \to \phi\mu^+\mu^-$ decay

In the SM, the double differential branching ratio $\frac{d^2\mathcal{B}}{d\hat{s}d\hat{u}}$ for $B_s \to \phi\mu^+\mu^-$ may be written as [18]

$$
\begin{aligned}
\frac{d^2\mathcal{B}^{SM}}{d\hat{s}d\hat{u}} =\ & \tau_B \frac{G_F^2 \alpha_e^2 m_{B_s}^5}{2^{11}\pi^5} |V_{ts}^* V_{tb}|^2 \\
& \times \Bigg\{ \frac{|A|^2}{4}\Big(\hat{s}(\lambda + \hat{u}^2) + 4\hat{m}_\mu^2 \lambda\Big) + \frac{|E|^2}{4}\Big(\hat{s}(\lambda + \hat{u}^2) - 4\hat{m}_\mu^2 \lambda\Big) \\
& + \frac{1}{4\hat{m}_\phi^2}\Big[|B|^2\Big(\lambda - \hat{u}^2 + 8\hat{m}_\phi^2(\hat{s} + 2\hat{m}_\mu^2)\Big) + |F|^2\Big(\lambda - \hat{u}^2 + 8\hat{m}_\phi^2(\hat{s} - 4\hat{m}_\mu^2)\Big)\Big] \\
& - 2\hat{s}\hat{u}\Big[Re(BE^*) + Re(AF^*)\Big] \\
& + \frac{\lambda}{4\hat{m}_\phi^2}\Big[|C|^2(\lambda - \hat{u}^2) + |G|^2\Big(\lambda - \hat{u}^2 + 4\hat{m}_\mu^2(2 + 2\hat{m}_\phi^2 - \hat{s})\Big)\Big] \\
& - \frac{1}{2\hat{m}_\phi^2}\Big[Re(BC^*)(1 - \hat{m}_\phi^2 - \hat{s})(\lambda - \hat{u}^2) \\
& \qquad + Re(FG^*)\Big((1 - \hat{m}_\phi^2 - \hat{s})(\lambda - \hat{u}^2) + 4\hat{m}_\mu^2 \lambda\Big)\Big] \\
& - 2\frac{\hat{m}_\mu^2}{\hat{m}_\phi^2}\lambda\Big[Re(FH^*) - Re(GH^*)(1 - \hat{m}_\phi^2)\Big] + |H|^2\frac{\hat{m}_\mu^2}{\hat{m}_\phi^2}\hat{s}\lambda \Bigg\},
\end{aligned}
\tag{3}
$$

where $p = p_B + p_\phi$, $s = q^2$ and $q = p_+ + p_-$ ($p_\pm$ the four-momenta of the muons), and the auxiliary functions $A - H$ can be found in Ref. [18]. The hat denotes normalization in terms of the B-meson mass, m_{B_s}, e.g. $\hat{s} = s/m_{B_s}^2$, $\hat{m}_q = m_q/m_{B_s}$.

In the MSSM without R-parity, the double differential branching ratio including the squark exchange contribution could be gotten from Eq. (3) by the replacements [19]

$$
\begin{aligned}
A(\hat{s}) &\to A(\hat{s}) + \frac{1}{W}\left[\frac{2V^{B_s\to\phi}(\hat{s})}{m_{B_s} + m_\phi}m_{B_s}^2\right]\sum_i \frac{\lambda'_{2i2}\lambda'^*_{2i3}}{8m_{\tilde{u}_{iL}}^2}, \\
B(\hat{s}) &\to B(\hat{s}) + \frac{1}{W}\left[-(m_{B_s} + m_\phi)A_1^{B_s\to\phi}(\hat{s})\right]\sum_i \frac{\lambda'_{2i2}\lambda'^*_{2i3}}{8m_{\tilde{u}_{iL}}^2}, \\
C(\hat{s}) &\to C(\hat{s}) + \frac{1}{W}\left[\frac{A_2^{B_s\to\phi}(\hat{s})}{m_{B_s} + m_\phi}m_{B_s}^2\right]\sum_i \frac{\lambda'_{2i2}\lambda'^*_{2i3}}{8m_{\tilde{u}_{iL}}^2}, \\
D(\hat{s}) &\to D(\hat{s}) + \frac{1}{W}\left[\frac{2m_\phi}{\hat{s}}\Big(A_3^{B_s\to\phi}(\hat{s}) - A_0^{B_s\to\phi}(\hat{s})\Big)\right]\sum_i \frac{\lambda'_{2i2}\lambda'^*_{2i3}}{8m_{\tilde{u}_{iL}}^2},
\end{aligned}
$$

3

$$
\begin{aligned}
E(\hat{s}) &\rightarrow E(\hat{s}) - \frac{1}{W}\left[\frac{2V^{B_s\to\phi}(\hat{s})}{m_{B_s}+m_\phi}m_{B_s}^2\right]\sum_i \frac{\lambda'_{2i2}\lambda'^*_{2i3}}{8m_{\tilde{u}_{iL}}^2}, \\
F(\hat{s}) &\rightarrow F(\hat{s}) - \frac{1}{W}\left[-(m_{B_s}+m_\phi)A_1^{B_s\to\phi}(\hat{s})\right]\sum_i \frac{\lambda'_{2i2}\lambda'^*_{2i3}}{8m_{\tilde{u}_{iL}}^2}, \\
G(\hat{s}) &\rightarrow G(\hat{s}) - \frac{1}{W}\left[\frac{A_2^{B_s\to\phi}(\hat{s})}{m_{B_s}+m_\phi}m_{B_s}^2\right]\sum_i \frac{\lambda'_{2i2}\lambda'^*_{2i3}}{8m_{\tilde{u}_{iL}}^2}, \\
H(\hat{s}) &\rightarrow H(\hat{s}) - \frac{1}{W}\left[\frac{2m_\phi}{\hat{s}}\left(A_3^{B_s\to\phi}(\hat{s})-A_0^{B_s\to\phi}(\hat{s})\right)\right]\sum_i \frac{\lambda'_{2i2}\lambda'^*_{2i3}}{8m_{\tilde{u}_{iL}}^2},
\end{aligned}
\tag{4}
$$

where $W = -\frac{G_F\alpha_e}{2\sqrt{2}\,\pi}V_{ts}^*V_{tb}m_{B_s}$.

The sneutrino exchange contributions are summarized as

$$
\begin{aligned}
\frac{d^2\mathcal{B}^{\tilde{\nu}}}{d\hat{s}d\hat{u}} &= \tau_B\frac{m_{B_s}^3}{2^7\pi^3}\Bigg\{-\frac{\hat{m}_\mu^2}{\hat{m}_\phi^2}\bigg[Im(WB\mathcal{T}_S^*)\Big(\lambda^{-\frac{1}{2}}\hat{u}(1-\hat{m}_\phi^2-\hat{s})\Big) \\
&\quad +Im(WC\mathcal{T}_S^*)\lambda^{\frac{1}{2}}\hat{u} - Im(WF\mathcal{T}_P^*)\lambda^{\frac{1}{2}} \\
&\quad +Im(WG\mathcal{T}_P^*)\lambda^{\frac{1}{2}}(1-\hat{m}_\phi^2)\bigg] + |\mathcal{T}_S|^2(\hat{s}-2\hat{m}_\mu^2)\Bigg\},
\end{aligned}
\tag{5}
$$

with

$$
\begin{aligned}
\mathcal{T}_S &= \left[\frac{i}{2}\frac{A_0^{B\to\phi}(\hat{s})}{\overline{m}_b+\overline{m}_s}\lambda^{\frac{1}{2}}m_{B_s}^2\right]\sum_i\left(\frac{\lambda_{i22}^*\lambda'_{i32}}{8m_{\tilde{\nu}_{iL}}^2}-\frac{\lambda_{i22}\lambda'^*_{i23}}{8m_{\tilde{\nu}_{iL}}^2}\right), \\
\mathcal{T}_P &= \left[\frac{i}{2}\frac{A_0^{B\to\phi}(\hat{s})}{\overline{m}_b+\overline{m}_s}\lambda^{\frac{1}{2}}m_{B_s}^2\right]\sum_i\left(\frac{\lambda_{i22}^*\lambda'_{i32}}{8m_{\tilde{\nu}_{iL}}^2}+\frac{\lambda_{i22}\lambda'^*_{i23}}{8m_{\tilde{\nu}_{iL}}^2}\right).
\end{aligned}
\tag{6}
$$

In the MSSM with R-parity, all the effects arise from the RPC MIs contributing to $C_7, \widetilde{C}_9^{eff}, \widetilde{C}_{10}$, and they are

$$
\begin{aligned}
C_7^{RPC} &= C_7^{Diag} + C_7^{MI} + nC_7'^{MI}, \\
(C_9^{eff})^{RPC} &= (\widetilde{C}_9^{eff})^{Diag} + (\widetilde{C}_9^{eff})^{MI} + n(C_9'^{eff})^{MI}, \\
C_{10}^{RPC} &= \widetilde{C}_{10}^{Diag} + \widetilde{C}_{10}^{MI} + nC_{10}'^{MI},
\end{aligned}
\tag{7}
$$

where $n=1$ for the terms related to the form factors V and T_1 as well as $n=-1$ for the terms related to the form factors A_0, A_1, A_2, T_2 and T_3 in $B_s\to\phi\mu^+\mu^-$ decay. $C_7^{Diag,MI}, (\widetilde{C}_9^{eff})^{Diag,MI}, \widetilde{C}_{10}^{Diag,MI}$, $C_7'^{MI}, (C_9'^{eff})^{MI}$ and $C_{10}'^{MI}$ have been estimated in Refs. [20–22]. The results for $\mathcal{B}(B_s\to\phi\mu^+\mu^-)$ including MI effects can be obtained from Eq. (3) by the following replacements [9, 23]:

$$
\begin{aligned}
C_7^{SM} &\rightarrow C_7^{SM} + C_7^{RPC}, \\
(C_9^{eff})^{SM} &\rightarrow (C_9^{eff})^{SM} + (C_9^{eff})^{RPC}, \\
C_{10}^{SM} &\rightarrow C_{10}^{SM} + C_{10}^{RPC}.
\end{aligned}
\tag{8}
$$

From the double differential branching ratio, we can get the dimuon forward-backward asymmetry [18]

$$\mathcal{A}_{FB}(B_s \to \phi\mu^+\mu^-) = \int d\hat{s} \, \frac{\int_{-1}^{+1} \frac{d^2\mathcal{B}(B_s \to \phi\mu^+\mu^-)}{d\hat{s}dcos\theta} sign(cos\theta)dcos\theta}{\int_{-1}^{+1} \frac{d^2\mathcal{B}(B_s \to \phi\mu^+\mu^-)}{d\hat{s}dcos\theta} dcos\theta}. \tag{9}$$

3 Numerical results and analyses

In this section, we will investigate the above mentioned physics observables and study their sensitivity to the new effects due to the MSSM with and without R-parity. When we study the SUSY effects, we consider only one new coupling at one time, neglecting the interferences between different new couplings, but keeping their interferences with the SM amplitude. The input parameters are collected in Appendix, and the following experimental data will be used to constrain parameters of the relevant new couplings [2, 8, 17]

$$\mathcal{B}(B_s \to \mu^+\mu^-) < 4.5 \times 10^{-9} \text{ (at 95\% CL)},$$

$$\mathcal{B}(B \to K\mu^+\mu^-) = (0.48 \pm 0.06) \times 10^{-6},$$

$$\mathcal{B}(B \to K^*\mu^+\mu^-) = (1.15 \pm 0.15) \times 10^{-6},$$

$$\mathcal{B}(B_s \to \phi\mu^+\mu^-) = (1.47 \pm 0.52) \times 10^{-6}. \tag{10}$$

To be conservative, we use the input parameters varied randomly within 1σ error bar and the experimental bounds at 95% CL in our numerical results.

3.1 The RPV MSSM effects

Firstly, we consider the RPV effects in $B_s \to \phi\mu^+\mu^-$ decay. There are three RPV coupling products, which are $\lambda'_{2i2}\lambda'^*_{2i3}$ due to squark exchange as well as $\lambda_{i22}\lambda'^*_{i23}$ and $\lambda^*_{i22}\lambda'_{i32}$ due to sneutrino exchange, relevant to $B_s \to \mu^+\mu^-$, $B_s \to \phi\mu^+\mu^-$ and $B \to K^{(*)}\mu^+\mu^-$ decays. We combine the experimental bounds in Eq. (10) at 95% CL to constrain the three RPV coupling products. Comparing with the bounds obtained in Ref. [16], we find that $\lambda_{i22}\lambda'^*_{i23}$ and $\lambda^*_{i22}\lambda'_{i32}$ couplings are further constrained by new upper limit of $\mathcal{B}(B_s \to \mu^+\mu^-)$, and we obtain $|\lambda_{i22}\lambda'^*_{i23}, \lambda^*_{i22}\lambda'_{i32}| \leq 1.3 \times 10^{-4}$.

Using the constrained parameter spaces from the experimental data in Eq. (10), we turn to analysis the constrained RPV effects on the observables of $B_s \to \phi\mu^+\mu^-$ decay which have not been measured yet. The s-channel sneutrino exchange couplings $\lambda_{i22}\lambda'^*_{i23}$ and $\lambda^*_{i22}\lambda'_{i32}$, which are strongly constrained

from $\mathcal{B}(B \to \mu^+\mu^-)$, have negligible contribution to $B_s \to \phi\mu^+\mu^-$ decay. The t-channel squark exchange coupling $\lambda'_{2i3}\lambda'^*_{2i2}$, which is mainly constrained from $\mathcal{B}(B \to K^*\mu^+\mu^-)$ and $\mathcal{B}(B_s \to \phi\mu^+\mu^-)$, has considerable contribution to $B_s \to \phi\mu^+\mu^-$. The effects of the constrained $\lambda'_{2i2}\lambda'^*_{2i3}$ in $B_s \to \phi\mu^+\mu^-$ are displayed in Fig. 1 by the two-dimensional scatter plots, and the SM predictions are also shown for comparing conveniently. The dimuon invariant mass distribution and the dimuon forward-backward asymmetry are given with vector meson dominance contribution excluded in terms of $d\mathcal{B}/d\hat{s}$ and $d\mathcal{A}_{FB}/d\hat{s}$, and included in $d\mathcal{B}'/d\hat{s}$ and $d\mathcal{A}'_{FB}/d\hat{s}$, respectively.
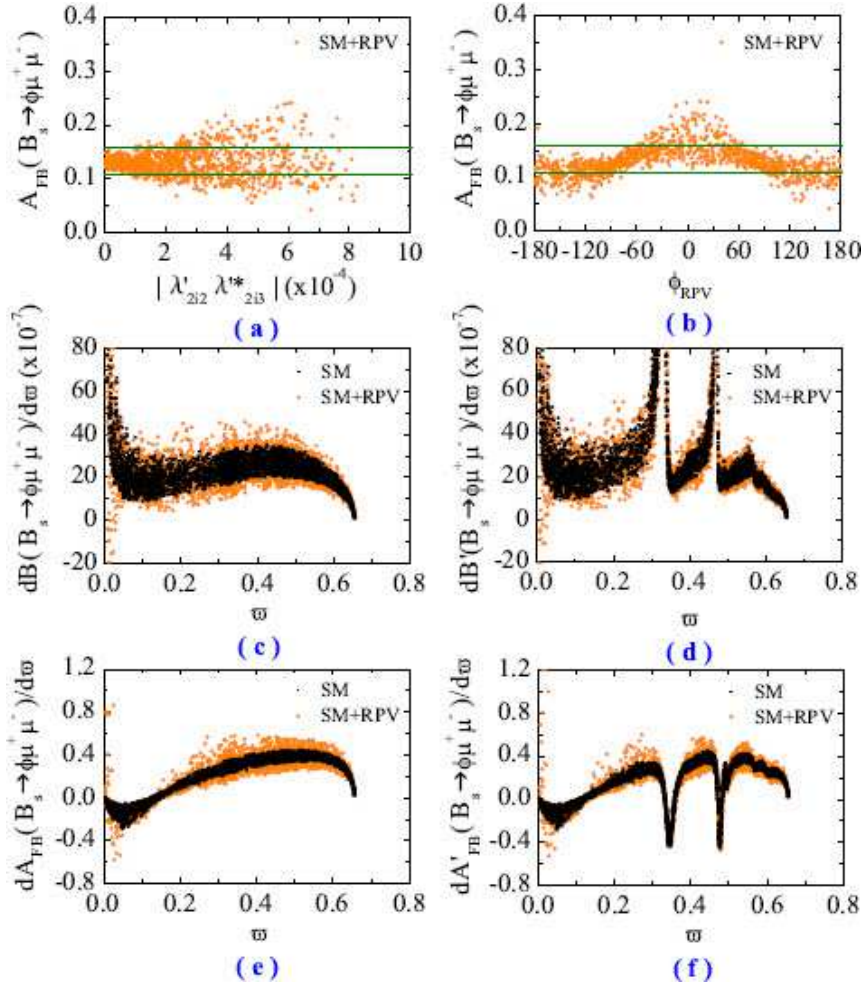

Figure 1: The effects of RPV coupling $\lambda'_{2i2}\lambda'^*_{2i3}$ due to the squark exchange in $B_s \to \phi\mu^+\mu^-$ decay. ϕ_{RPV} denotes the RPV weak phase of $\lambda'_{2i2}\lambda'^*_{2i3}$ and ϖ denotes $\hat{s}$. The limit of SM prediction is shown by olive horizontal solid lines in plot (a) and (b).

Now we discuss the plots of Fig. 1 in detail. Figs. 1 (a) and (b) show the constrained effects of the modulus and weak phase of $\lambda'_{2i2}\lambda'^*_{2i3}$ on $\mathcal{A}_{FB}(B_s \to \phi\mu^+\mu^-)$, respectively. One can see that such contributions could give large $\mathcal{A}_{FB}(B_s \to \phi\mu^+\mu^-)$ when $|\lambda'_{2i2}\lambda'^*_{2i3}|$ is large and corresponding $|\phi_{RPV}|$ is

near 0°. Figs. 1 (c-f) display the constrained RPV effects on the dimuon invariant mass spectrum and the differential forward-backward asymmetry, and we can see that the constrained $\lambda'_{2i2}\lambda'^{*}_{2i3}$ still has remarkable effects on them. As for the dimuon invariant mass spectrum, this observable has also been measured as a function of the dimuon invariant mass square q^2 by CDF [2]. We do not impose the experimental bound from $d\mathcal{B}'(B_s \to \phi\mu^+\mu^-)/d\hat{s}$ and leave it as prediction of the restricted parameter space of $\lambda'_{2i2}\lambda'^{*}_{2i3}$, and compare it with the experimental results in Ref. [2]. The measurement is basically consistent with the SM prediction. Nevertheless in the region of $2.00 < q^2 < 8.68$ (i.e. $0.07 < \hat{s} < 0.31$), the central value of the experimental data from CDF is smaller than one of its SM predictions. The prediction of $d\mathcal{B}'(B_s \to \phi\mu^+\mu^-)/d\hat{s}$ including $\lambda'_{2i2}\lambda'^{*}_{2i3}$ coupling is allowed by current experimental data, and the effects of $\lambda'_{2i2}\lambda'^{*}_{2i3}$ coupling may be further constrained if the experimental bound of the dimuon invariant mass spectrum in Ref. [2] is considered.

3.2   The RPC MI effects

Next, we explore the RPC MI effects in $B_s \to \phi\mu^+\mu^-$ decay in the MSSM with large $\tan\beta$. There are three kinds of MIs $(\delta^u_{LL})_{23}$, $(\delta^d_{LL})_{23}$ and $(\delta^d_{RR})_{23}$ contributing to $B_s \to \mu^+\mu^-$, $B \to K^{(*)}\mu^+\mu^-$ and $B_s \to \phi\mu^+\mu^-$ decays at the same time. The experimental data shown in Eq. (10) will be used to constrain these three kinds of MI parameters. Our bounds on the three MI couplings are demonstrated in Fig. 2. Compared with the bounds in Ref. [16], the allowed spaces of all three MI parameters are further constrained by the new upper limit of $\mathcal{B}(B_s \to \mu^+\mu^-)$.
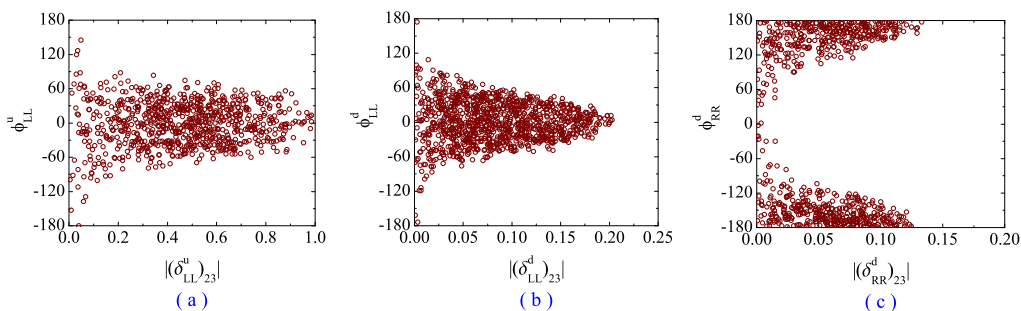

Figure 2: The allowed parameter spaces of $(\delta^u_{LL})_{23}$, $(\delta^d_{LL})_{23}$ and $(\delta^d_{RR})_{23}$ MI parameters constrained by $\mathcal{B}(B_s \to \mu^+\mu^-, \phi\mu^+\mu^-)$ and $\mathcal{B}(B \to K^{(*)}\mu^+\mu^-)$ at 95% CL, and the RPC phases are given in degree.

Then we analyze the RPC supersymmetric effects in $B_s \to \phi\mu^+\mu^-$ decay. Besides the MI contributions, the SUSY predictions also include the contributions that come from graphs including SUSY Higgs bosons and sparticles in the limit in which we neglect all the MI contributions,
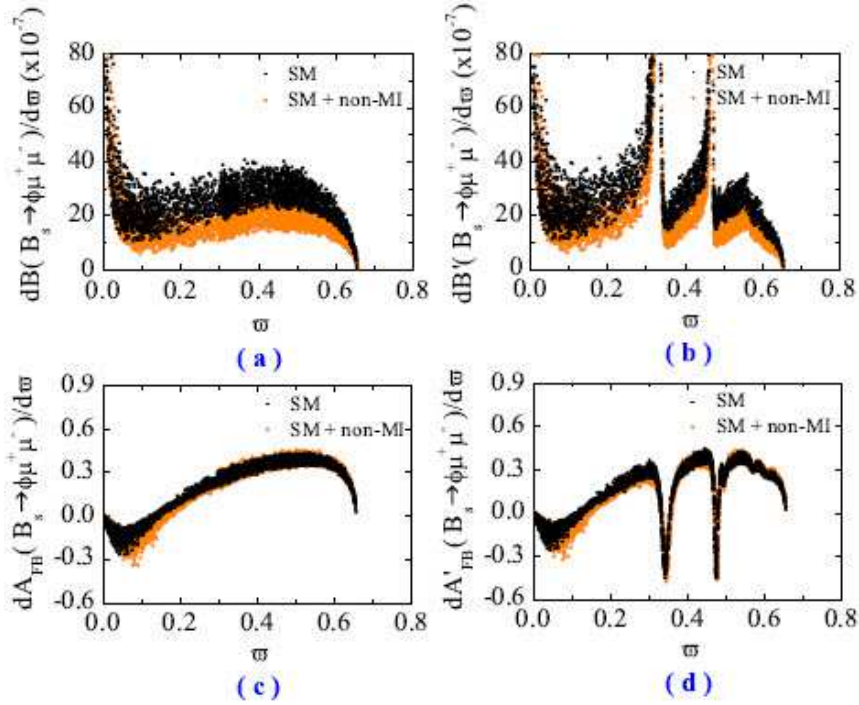
Figure 3: The constrained non-MI effects in $B_s \to \phi\mu^+\mu^-$ decay, and ϖ denotes $\hat{s}$.

which are called non-MI contributions. We find that non-MI couplings have negligible effect in $\mathcal{A}_{FB}(B_s \to \phi\mu^+\mu^-)$. The non-MI SUSY effects on the dimuon invariant mass spectrum and the differential forward-backward asymmetry of $B_s \to \phi\mu^+\mu^-$ are shown in Fig. 3. As shown in Figs. 3 (a-b), $d\mathcal{B}(B_s \to \phi\mu^+\mu^-)/d\hat{s}$ could be increased slightly in the low $\hat{s}$ region, but obviously decreased in the high $\hat{s}$ region. Figs. 3 (c-d) show us that the non-MI effects could slightly suppress $d\mathcal{A}_{FB}(B_s \to \phi\mu^+\mu^-)/d\hat{s}$ at the low $\hat{s}$ ranges.

Since the constrained $(\delta_{LL}^d)_{23}$ and $(\delta_{RR}^d)_{23}$ MIs have no obvious effects in $B_s \to \phi\mu^+\mu^-$, we only show the $(\delta_{LL}^u)_{23}$ MI contributions to $B_s \to \phi\mu^+\mu^-$ in Fig. 4. Note that the SUSY predictions in Fig. 4 also include the non-MI contributions shown in Fig. 3. From Figs. 4 (a-b), one can see that $\mathcal{A}_{FB}(B_s \to \phi\mu^+\mu^-)$ is very sensitive to $(\delta_{LL}^u)_{23}$ MI, and it increases with $|(\delta_{LL}^u)_{23}|$ but decreases with $|\phi_{LL}^u|$. Figs. 4 (c-d) show us $d\mathcal{B}(B_s \to \phi\mu^+\mu^-)/d\hat{s}$ is compatible with the theoretical uncertainties and thus is indistinguishable from its SM prediction. As shown in Figs. 4 (e-f), the constrained $(\delta_{LL}^u)_{23}$ MI effects on $d\mathcal{A}_{FB}(B_s \to \phi\mu^+\mu^-)/d\hat{s}$ could be significant. Note that the theoretical uncertainty of $d\mathcal{A}_{FB}(B_s \to \phi\mu^+\mu^-)/d\hat{s}$ including $(\delta_{LL}^u)_{23}$ MI is smaller than one of $d\mathcal{A}_{FB}(B \to K^*\mu^+\mu^-)/d\hat{s}$ in Ref. [16].
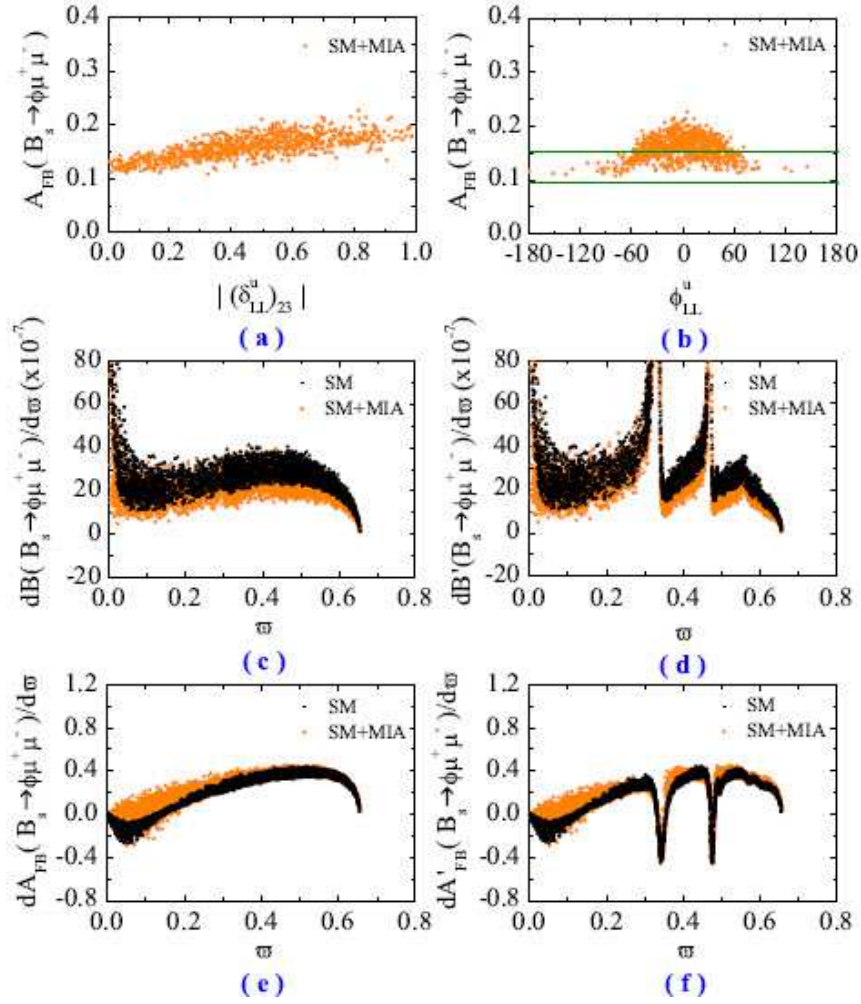
Figure 4: The constrained $(\delta_{LL}^u)_{23}$ MI effects in $B_s \to \phi\mu^+\mu^-$ decay, and ϖ denotes $\hat{s}$.

4   Conclusions

In this paper, we have studied $B_s \to \phi\mu^+\mu^-$ decay in the MSSM with and without R-parity. We have found that the bounds of sneutrino exchange RPV couplings as well as $(\delta_{LL}^u)_{23}$ and $(\delta_{LL,RR}^d)_{23}$ MI couplings are further constrained by the new experimental upper limit of $\mathcal{B}(B_s \to \mu^+\mu^-)$. The constrained RPV coupling due to t-channel squark exchange still has significant effects in $B_s \to \phi\mu^+\mu^-$ decay, and $\mathcal{A}_{FB}(B_s \to \phi\mu^+\mu^-)$ is sensitive to both the modulus and the weak phase of this RPV coupling product. The constrained $(\delta_{LL}^u)_{23}$ MI could give large effects on $\mathcal{A}_{FB}(B_s \to \phi\mu^+\mu^-)$ and $d\mathcal{A}_{FB}(B_s \to \phi\mu^+\mu^-)/d\hat{s}$ in all $\hat{s}$ region, and besides, $\mathcal{A}_{FB}(B_s \to \phi\mu^+\mu^-)$ is very sensitive to both $(\delta_{LL}^u)_{23}|$ and (ϕ_{LL}^u), but the constrained $(\delta_{LL}^u)_{23}$ MI has small effects on $d\mathcal{B}(B_s \to \phi\mu^+\mu^-)/d\hat{s}$. In addition, the constrained $(\delta_{LL,RR}^d)_{23}$ MIs have ignorable effects on the observables of $B_s \to \phi\mu^+\mu^-$ decay, nevertheless $d\mathcal{A}_{FB}(B_s \to \phi\mu^+\mu^-)/d\hat{s}$ could be distinctly decreased by the SUSY contributions

9

which come from graphs including SUSY Higgs bosons and sparticles in the limit in which we neglect all the MI contributions. More precise measurements at the LHCb and the future super-B factories could test our results and further shrink or reveal the parameter spaces of MSSM with and without R-parity.

Acknowledgments

Appendix: Input parameters

The input parameters are summarized in Table 1. For the RPC MI effects, we take the five free parameters $m_0 = 450\ GeV, m_{1/2} = 780\ GeV, A_0 = -1110$, sign$(\mu) > 0$ and $\tan\beta = 41$ from Ref. [25]. All other MSSM parameters are then determined according to the constrained MSSM scenario as implemented in the program package SUSPECT [26]. For the form factors involving the $B_s \to \phi$ transition, we will use the light-cone QCD sum rules (LCSRs) results [27, 28], which are renewed with radiative corrections to the leading twist wave functions and SU(3) breaking effects. For the q^2 dependence of the form factors, they can be parameterized in terms of simple formulae with two or three parameters. The expression can be found in Ref. [27, 28]. In our numerical data analysis, the uncertainties induced by $F(0)$ are also considered.

References

[1] T. Aaltonen *et al.* (CDF Collaboration), Phys. Rev. Lett. **106**, 161801 (2011).

[2] T. Aaltonen *et al.* (CDF Collaboration), Phys. Rev. Lett. **107**, 201802 (2011).

[3] T. Aaltonen *et al.* (CDF Collaboration), Phys. Rev. Lett. **107**, 191801 (2011).

[4] S. Chatrchyan *et al.* [CMS Collaboration], arXiv:1203.3976 [hep-ex].

Table 1: Default values of the input parameters.

$m_{B_s} = 5.370\ GeV, \quad m_{B_{u,d}} = 5.279\ GeV, \quad m_W = 80.425\ GeV, \quad m_\phi = 1.019\ GeV,$	
$m_{K^\pm} = 0.494\ GeV, \quad m_{K^0} = 0.498\ GeV, \quad m_{K^{*\pm}} = 0.892\ GeV, \quad m_{K^{*0}} = 0.896\ GeV,$	
$\overline{m}_b(\overline{m}_b) = (4.19^{+0.18}_{-0.06})\ GeV, \quad \overline{m}_s(2GeV) = (0.100^{+0.030}_{-0.020})\ GeV,$	
$\overline{m}_u(2GeV) = 0.0017 \sim 0.0031\ GeV, \quad \overline{m}_d(2GeV) = 0.0041 \sim 0.0057\ GeV,$	
$m_e = 0.511 \times 10^{-3}\ GeV, \quad m_\mu = 0.106\ GeV, \quad m_{t,pole} = 172.9 \pm 1.1\ GeV.$	[17]
$\tau_{B_s} = (1.466 \pm 0.059)\ ps, \quad \tau_{B_d} = (1.530 \pm 0.009)\ ps, \quad \tau_{B_u} = (1.638 \pm 0.011)\ ps.$	[17]
$|V_{tb}| \approx 0.99910, \quad |V_{ts}| = 0.04161^{+0.00012}_{-0.00078}.$	[17]
$\sin^2\theta_W = 0.22306, \quad \alpha_e = 1/137.$	[17]
$f_{B_s} = 0.230 \pm 0.030\ GeV.$	[24]

[5] R. Aaij *et al.* (LHCb Collaboration), arXiv:1112.0511 [hep-ex].

[6] R. Aaij *et al.* (LHCb Collaboration), Phys. Lett. **B699**, 330 (2011).

[7] The CMS and LHCb Collaborations, CMS-PAS-BPH-11-019, LHCb-CONF-2011-047, CERN-LHCb-CONF-2011-047.

[8] R. Aaij *et al.* (LHCb Collaboration), arXiv:1203.4493 [hep-ex].

[9] E. Lunghi and A. Soni, JHEP **1011**, 121 (2010).

[10] U. O. Yilmaz, Eur. Phys. J. **C58**, 555 (2008).

[11] S. M. Zebarjad, F. Falahati and H. Mehranfar, Phys. Rev. **D79**, 075006 (2009).

[12] Q. Chang and Y. -H. Gao, Nucl. Phys. **B845**, 179 (2011).

[13] Y. Li and J. Hua, Eur. Phys. J. **C71**, 1764 (2011).

[14] B. Dutta, Y. Mimura and Y. Santoso, Phys. Lett. **B706**, 188 (2011).

[15] C. Beskidt *et al.*, Phys. Lett. **B705**, 493 (2011).

[16] Ru-Min Wang, Yuan-Guo Xu, Yi-Long Wang and Ya-Dong Yang, arXiv:1112.3174 [hep-ph].

[17] K. Nakamura *et al.* (Particle Data Group), J. Phys. **G37**, 075021 (2010) and 2011 partial update for the 2012 edition.

[18] A. Ali, P. Ball, L. T. Handoko and G. Hiller, Phys. Rev. **D61**, 074024 (2000).

[19] Y. G. Xu, R. M. Wang and Y. D. Yang, Phys. Rev. **D74**, 114019 (2006).

[20] E. Lunghi, A. Masiero, I. Scimemi and L. Silvestrini, Nucl. Phys. **B568**, 120-144 (2000).

[21] P. L. Cho, M. Misiak and D. Wyler, Phys. Rev. **D54**, 3329-3344 (1996).

[22] J. L. Hewett and J. D. Wells, Phys. Rev. D **55**, 5549 (1997).

[23] W. Altmannshofer *et al.*, JHEP **0901**, 019 (2009).

[24] S. Hashimoto, Int. J. Mod. Phys. **A20**, 5133-5144 (2005).

[25] S. Heinemeyer, arXiv:1202.1991 [hep-ph].

[26] A. Djouadi, J. L. Kneur and G. Moultaka, Comput. Phys. Commun. **176**, 426 (2007).

[27] P. Ball and R. Zwicky, Phys. Rev. **D71**, 014015 (2005).

[28] P. Ball and R. Zwicky, Phys. Rev. **D71**, 014029 (2005).